Flow Turbulence Combust (2014) 93:37–61
DOI 10.1007/s10494-014-9533-9

A Bypass Transition Model Based on the Intermittency Function

Xuan Ge · Sunil Arolla · Paul Durbin

Received: 10 November 2013 / Accepted: 7 February 2014 / Published online: 27 April 2014

Abstract An intermittency model that is formulated in local variables is proposed for representing bypass transition in Reynolds-Averaged Navier-Stokes (RANS) computations. No external data correlation is used to fix transition. Transition is initiated by diffusion, and a source term carries it to completion. A sink term is created to predict the laminar region before transition, then it vanishes in the turbulent region. Both the source and sink are functions of a wall-distance Reynolds number and turbulence scale. A modification is introduced to predict transition in separated boundary layers. The transition model is incorporated with the $k-\omega$ RANS model. The present model is implemented into a general purpose, computational fluid dynamics (CFD) code. The model is validated with several test cases. Decent agreement with the available data is observed in a range of flows.

Keywords Laminar to turbulent transition · Intermittency · Bypass transition · Reynolds averaged modeling

1 Introduction

1.1 Challenge of modeling laminar to turbulent transition

While RANS models for a wide range of fully turbulent flows are available in general CFD codes, models for laminar-to-turbulent transition are far more limited. One of the difficulties is that transition takes place through different mechanisms in various engineering flows. When free-stream turbulence level ($\sqrt{2k/3}/U_{ref}$) is about 1% or more, the boundary layers proceed from laminar to fully turbulent without the occurrence of linear instability of the base state [5]. This mode of transition is referred to as bypass transition. Turbulence diffuses

X. Ge · P. Durbin (✉)
Aerospace Engineering, Iowa State University, Ames, IA, USA
e-mail: durbin@iastate.edu

S. Arolla
Aerospace Engineering, Cornell University, Ithaca, NY, USA

into the laminar boundary layer, and generates disturbances known as Klebanoff modes. These grow in amplitude, and transition to turbulence occurs. [4]. In separation-induced transition, a laminar boundary layer separates under the influence of a pressure gradient and transition occurs within the separated shear layer due to the inflection point instability. It is difficult to develop a model which is valid for these different mechanisms. For general use in CFD, the model must be formulated in local variables, eschewing dependency on the boundary layer thickness or free-stream turbulence.

1.2 Brief introduction to intermittency based models

One method to model the Reynolds averaged effect of bypass transition for practical flow prediction is to use the concept of intermittency γ to blend the flow from the laminar to the turbulent regions. Initially, [1] correlated experimental data and prescribed an intermittency distribution across the transition. But it was not clear, in general, how to predict the transition location, or how to adapt the function to general flows.

Steelant and Dick [11] proposed a transport equation for intermittency, in which the source term of the equation was developed such that the γ distribution of [1] can be reproduced. But it was restricted to boundary layer computations. More importantly, it did not predict transition: a data correlation in terms of boundary layer momentum thickness and free-stream turbulence did that. The momentum thickness is an integral property and free-stream turbulence is a remote variable. [13] proposed an extended version of the [11] model, still requiring a data correlation. Correlations for both attached and separated flow were proposed, again not in terms of local parameters. This is unsuitable for general use in CFD.

With that motivation, [5] and [9] formulated a model in only local variables, known at each point of the flow. In their method, the data correlation is replaced by a transport equation for transition Reynolds number. A data correlation appears as a source in that Reynolds number transport equation; hence it is referred to as a correlation-based model [6]. The intermittency function γ solves a second transport equation. This is commonly called the $\gamma - R_t$ model.

The present objective is to develop a local model that invokes only one transport equation, for the intermittency γ. In this new method, no data correlation is invoked.

The present approach remains quite empirical, but the number of coefficients is fewer, and the role of each more apparent. The current model addresses bypass transition both in attached and separated flow. Although separation-induced transition proceeds by a different mechanism from attached flow transition, some measure has been taken to locate the separation and trigger transition at the proper location. The present γ equation is formulated for the $k - \omega$ RANS closure.

1.3 Rational of the current model

A data correlation given by [10] shows that

$$\Theta^2_{transition} = 0.07 \frac{\nu \lambda_\infty}{u'_\infty}. \tag{1.1}$$

$\Theta_{transition}$ is the momentum thickness at transition. λ_∞ is referred to as the free-stream integral length scale, and u' the magnitude of the streamwise velocity fluctuation. The data cover a wide range of pressure gradients, Reynolds numbers, free-stream turbulence

intensities and length scales. They were collapsed by (1.1) independently of all other parameters. Praisner and Clark [10] cite $C_\mu\omega = u'/\lambda$ for the $k-\omega$ model. Then (1.1) becomes

$$\Theta^2_{transition} = \frac{7\nu}{9\omega_\infty}. \tag{1.2}$$

Only the time scale of the free-stream turbulence is involved in this correlation. That seems too simple; but what is most interesting, is that just turbulence scale, and not pressure gradients or other parameters appear in (1.2). Turbulence scale enters the free-stream eddy viscosity k_∞/ω_∞ and the dissipation rate $C_\mu k_\infty \omega_\infty$.

In the present model, the value of γ varies from unity within free-stream turbulent flow to zero in the laminar boundary layer. The function γ is used to suppress production of the turbulent kinetic energy. Bypass transition is initiated through the diffusion of free-stream disturbances into the boundary layer. As γ rises from zero toward unity within the boundary layer, production of γ switches on and the eddy viscosity rises. Meanwhile, in order to have the laminar boundary layer before transition, a sink term is invoked within the boundary layer ; it drives γ towards zero. This model was originally proposed in [3]. That formulation was deficient in the sink term, and was only tested by boundary layer computations. It contained no method to represent transition in separated flow.

2 Formulation of the Model

The current model starts from the basic model of [3]. The intermittency transport equation is of the form

$$\frac{D\gamma}{Dt} = \partial_j\left[\left(\frac{\nu}{\sigma_l} + \frac{\nu_T}{\sigma_\gamma}\right)\partial_j\gamma\right] + F_\gamma|\Omega|\left(\gamma_{max} - \gamma\right)\sqrt{\gamma}. \tag{2.1}$$

with the boundary conditions $\gamma = 1$ in the free-stream and $\partial_n\gamma = 0$ on walls. $|\Omega|$ is the mean vorticity. An assessment of this initial approach showed nice agreement with experimental data in flat plate cases, both with and without pressure gradient. The model does not depend explicitly on the pressure gradient, which is consistent with the fact that turbulence closures generally do not depend directly on the pressure gradient.

The formulation (2.1) applied only to attached flow and was implemented only into a boundary layer code. In order to extend its application to general CFD codes and hence to predict more practical engineering flows, some changes have been made.

Consider an intermittency transport equation as follows [11]

$$\frac{D\gamma}{Dt} = \partial_j\left[\left(\frac{\nu}{\sigma_l} + \frac{\nu_T}{\sigma_\gamma}\right)\partial_j\gamma\right] + P_\gamma - E_\gamma. \tag{2.2}$$

The source term is in the same form as (2.1),

$$P_\gamma = F_\gamma|\Omega|\left(\gamma_{max} - \gamma\right)\sqrt{\gamma}. \tag{2.3}$$

The sink term is defined as,

$$E_\gamma = G_\gamma F_{turb}|\Omega|\gamma^{1.5}. \tag{2.4}$$

All the factors and constants will be explained in the following sections.

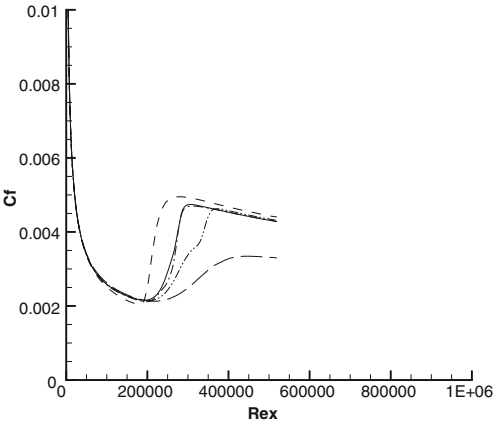

Fig. 1 Sensitivity of the transition location to σ_γ. $\sigma_\gamma = 0.2$ (solid), $\sigma_\gamma = 0.02$ (dash), $\sigma_\gamma = 0.1$ (dash-dot), $\sigma_\gamma = 0.4$ (dash-dotdot), $\sigma_\gamma = 0.8$ (long-dash)

2.1 Diffusion term

The two constants σ_l and σ_γ are set to 5.0 and 0.2, respectively. From the diffusion term itself, we can predict that increasing σ_γ decreases turbulent diffusivity and delays transition, and vice versa. In the current model, σ_γ is selected to be 0.2: if it is doubled or more, the diffusion is suppressed and the transition delayed. The model is less sensitive to this parameter once it becomes less than 0.2. When σ_γ is halved, the result changes very slightly; but it does give obvious early transition when σ_γ is 0.02 or even smaller. This is due to the sink term, which is designed to drive γ to zero in order to have a laminar region before transition. After transition, the sink vanishes and hence doubling the value of σ_γ delays the transition significantly. See Fig. 1, where skin friction coefficient (C_f) curves are plotted along the stream-wise direction of a flat plate. The conditions are those of T3A — one of the T3 series of flat-plate experiments conducted by the European Research Community on Flow Turbulence and Combustion (ERCOFTAC) [6].

However, the effect of σ_l is a bit subtle. When it is doubled, the C_f curve transitions early; whereas, transition occurs further downstream if σ_l is halved — the reverse effect of σ_γ (see Fig. 2). Durbin [3] attributes this to alteration of the mean shear in the upper part of the boundary layer.

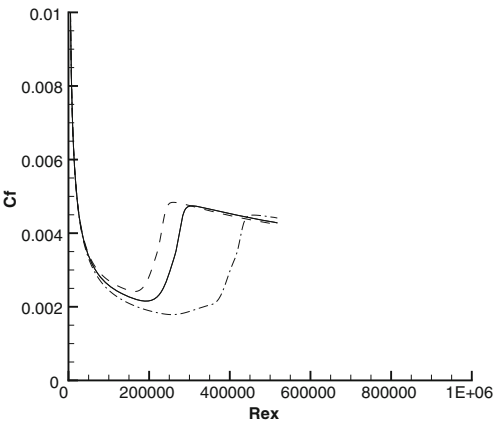

Fig. 2 Sensitivity of the transition location to σ_l. $\sigma_l = 5.0$ (solid), $\sigma_l = 10.0$ (dash), $\sigma_l = 2.5$ (dash-dot)

2.2 Source term

Note that $\gamma_{max} = 1.1$ instead of unity is placed in the source term. This is in order to enhance the effect of the source term to drive γ to 1. After each step of the computation, γ is forced to the value of $\min(\gamma, 1)$ to prevent values greater than unity. This has a small effect, but it does force a full transition to turbulence, guaranteeing γ to be unity after transition.

Mean shear is represented by the magnitude of the mean rotation rate $|\Omega|$, defined as $\sqrt{2 \cdot \Omega_{ij}\Omega_{ji}}$. It recalls that turbulence is caused by mean shear. $|\Omega|$ is an invariant measure of shear, and it vanishes in the irrotational free-stream.

The factor F_γ is a function of two parameters, R_v and T_ω. F_γ switches on as transition proceeds. Once it comes into play, γ will be driven up to unity within the region that F_γ affects. This causes turbulent kinetic energy k, as well as the eddy viscosity, to rise. Meanwhile, the sink term vanishes and the transition model becomes fully turbulent

Three non-dimensional parameters are involved,

$$\left.\begin{aligned} R_t &\equiv \frac{\nu_T}{\nu}, \\ T_\omega &\equiv R_t \frac{|\Omega|}{\omega}, \\ R_v &\equiv \frac{d^2|\Omega|}{2.188\nu}. \end{aligned}\right\} \tag{2.5}$$

where d is distance to the wall. R_t is the ratio of eddy viscosity to molecular viscosity, namely the turbulent Reynolds number. The parameter T_ω is R_t multiplied by $|\Omega|/\omega$ to make it vanish in the free-stream. Another view of T_ω is that in parallel flow $T_\omega = |\overline{uv}|/\nu\omega$. In the log-layer it equals to $u_*^2/\nu\omega = 1/\omega_+$.

R_v is the vorticity Reynolds number, which depends only on local variables. Near a wall it goes like wall distance squared, i.e. $R_v \to y_+^2/2.188$, as $y_+ \to 0$. It is defined such that, in the Blasius boundary layer, its maximum in the wall normal direction equals the momentum thickness Reynolds number: $\max_y R_v = R_\theta$. When the boundary layer is subjected to pressure gradients, the relationship between momentum thickness and vorticity Reynolds number will change: in Falkner-Skan boundary layers $\max_y R_v$ is less than R_θ for favorable pressure gradients and greater than R_θ for adverse pressure gradients. So a fixed value of R_v will correspond to a higher R_θ for favorable pressure gradients and a lower R_θ as the pressure gradient becomes adverse.

Langtry and Menter [6] stated a physical reason for using R_v, arguing that the combination $y^2|\Omega|$ is responsible for the growth of disturbances inside a boundary layer, while ν is responsible for their damping. To be concise, R_v implicitly contains information on R_θ. R_θ is used to indicate the onset of transition in data correlations.

Now come back to the definition of F_γ. T_ω is used to form a critical Reynolds number, R_c. It is a decreasing function of T_ω. If the turbulence intensity is low, T_ω will be low and R_c will be high. R_c is set as a linear ramp down between 400 and 40:

$$R_c = 400 - 360 \min\left(\frac{T_\omega}{2}, 1\right). \tag{2.6}$$

As the local Reynolds number R_v crosses R_c from below, F_γ ramps up from zero. Again a linear ramp up is used. A ramp down is added if the Reynolds number crosses

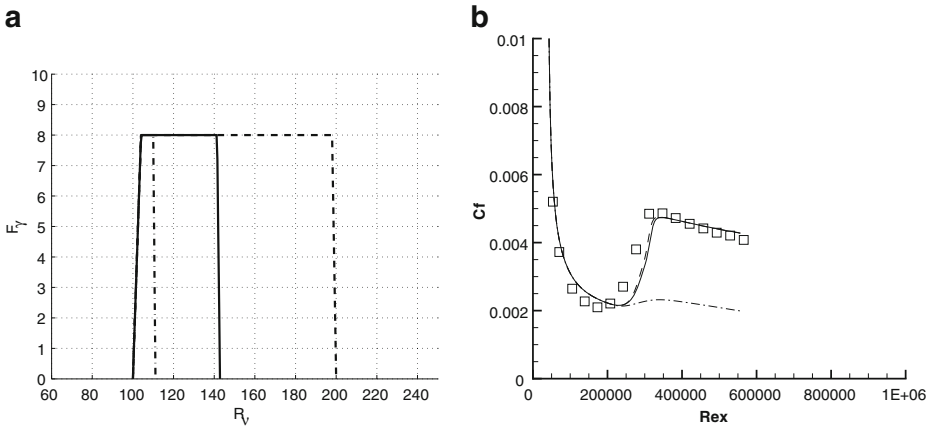

F_γ vs. R_ν with $R_c = 100$. C_f with different $R_{\nu bound}$

Fig. 3 R_{vbound} is equal to 100/0.5 (dash); 100/0.7 (solid);100/0.9 (dash-dot)

$R_{vbound} = 100/0.7$ without the flow becoming turbulent. This approach is used to suppress F_γ for low free-stream turbulence. The concrete formula for F_γ is

$$\begin{aligned} F_\gamma &= 2 \max\left[0, \min\left(100 - 0.7R_v, 1\right)\right] \\ &\quad \times \min\left[\max\left(R_v - R_c, 0\right), 4\right]. \end{aligned} \tag{2.7}$$

In other words,

$$F_\gamma = \begin{cases} 0, & if\ R_v \leqslant R_c,\ or\ if\ R_v \geqslant 100/0.7, \\ 8, & if\ R_v > R_c + 4\ and\ R_v \leqslant 100/0.7 - 1. \end{cases}$$

Note that this is a recalibration of the formulas in [3] because of the addition of E_γ to Eq. (2.2). The specific upper limit of 4 in the second factor of the right-hand side of Eq. (2.7) has small effect; a greater value does not change the result very much. A plot of F_γ versus R_v is given in Fig. 3, when the critical Reynolds number R_c is 100, which illustrates how F_γ ramps up then down. The upper limit of R_v where F_γ crosses from non-zero to zero (R_{vbound}) influences the location of transition. If it is set to be greater than 100/0.7, transition is accelerated; if it is less, transition is delayed. However, due to the effect of the sink term discussed in the next section, if for example $R_{vbound} = 100/0.5$ is used, the C_f curve will be barely changed rather than showing an early transition. However, when $R_{vbound} = 100/0.9$ transition is greatly delayed; see Fig. 3.

2.3 Sink term

Without a sink term, the γ-equation (2.2) would have the solution $\gamma \equiv 1$. The numerical elliptic solver will converge to unity within the whole domain, which will produce fully turbulent results. As illustrated in Fig. 4, when the sink is omitted the transition model has no effect.

In order to force γ close to zero within the laminar region, a sink term is added in Eq. (2.2). Another feature of the sink term is that it has to vanish after transition because γ is supposed to be unity in the fully turbulent region. This feature is implemented by the

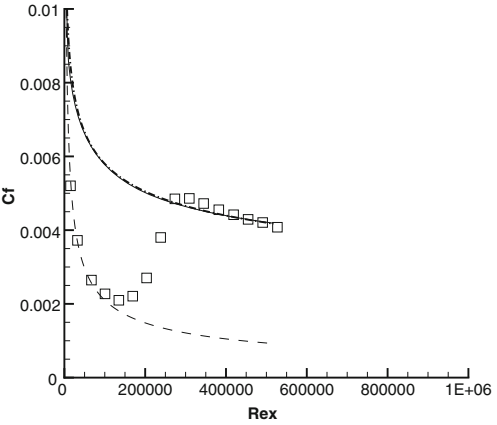

Fig. 4 Skin friction coefficient vs. Re_x on a flat plate (T3A): the solid curve results when the model is solved without the sink term. Experimental data (square), the theoretical laminar (dash) solution, and a turbulent data correlation (dash-dot) are also shown.

multiplication of two functions, G_γ and F_{turb}. This differs from the form invoked by [5] because we found that the sink term in the $\gamma - R_t$ model does not shut off in the fully turbulent region; hence, γ remains very small near the wall, even after transition.

The definition of G_γ is similar to F_γ in the source term, as defined in Eq. (2.8). It is used to ensure the laminar region before transition. It starts to ramps up at $R_v = 18$ and ramps down after $R_v = 100$. See Fig. 5. A factor 7.5 in (2.8) is chosen for the strength of the sink term.

$$G_\gamma = 7.5 \max\left[0, \min\left(100 - R_v, 1\right)\right] \times \min\left[\max\left(R_v - 18, 0\right), 1\right]. \tag{2.8}$$

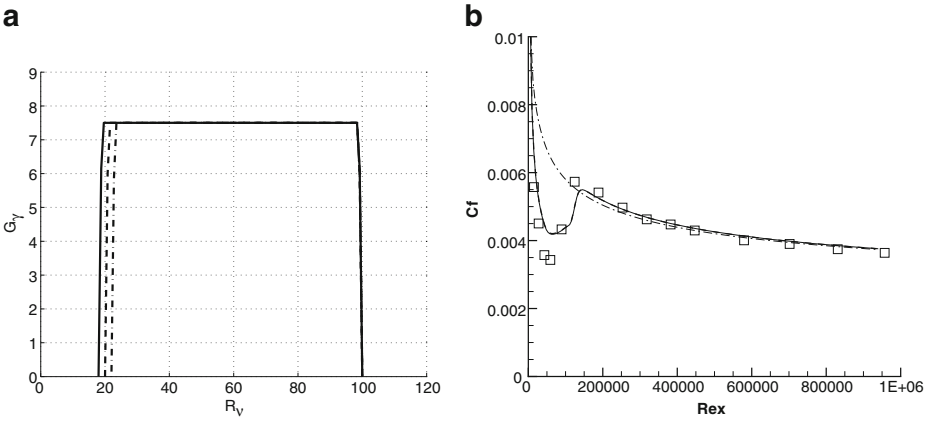

G_γ vs. R_ν. C_f with different $R_{\nu lbound}$.

Fig. 5 $R_{vlbound}$ is equal to 18 (solid); 22 (dash); 26 (dash-dot). From 18 to 22, the difference is tiny; but from 22 to 26, C_f suddenly becomes fully turbulent

In other words,

$$G_\gamma = \begin{cases} 0, & if\ R_v \leqslant 18,\ or\ if\ R_v \geqslant 100, \\ 7.5, & if\ R_v > 19\ and\ R_v \leqslant 99. \end{cases}$$

The lower bound $R_{vlbound} = 18$ is critical, to some extent. In the test case T3B [6], with high free-stream turbulence intensity, the model will be invalid if $R_{vlbound}$ too large. For such a case, the laminar region is thin and short. Therefore, a relatively high $R_{vlbound}$ may not catch the thin laminar region near the wall and hence the sink term may vanish. See Fig. 5b. Too small a value for $R_{vlbound}$ is not proper either because the sink term is supposed to vanish after transition. Recall that R_v goes like y_+^2 near the wall; hence, too small $R_{vlbound}$, say 0, makes G_γ non-zero near the wall, even in turbulent flow, with the sink term not vanishing.

F_{turb} is a function of R_v and R_t. It will vanish outside the laminar boundary layer. It is defined as,

$$F_{turb} = e^{-(R_v R_t)^{1.2}}. \tag{2.9}$$

The power 1.2 is selected to match data. A large value of it will reduce the region affected by F_{turb}, which in turn suppresses the sink and leads to early transition.

2.4 Separation modification

When a laminar boundary layer approaches separation, inflection point instability becomes a cause of transition. In this mechanism, an instability wave serves as the precursor to transition, and the phenomenology is different from bypass transition. However, free-stream turbulence can promote break down of instability waves into turbulence [16].

[5] pointed out that when separated flow transition was involved, their model (without modification for separation) would predict the turbulent reattachment location too far downstream. The same issue happens to the present model. And in some cases the reattachment may not occur at all. Low turbulent kinetic energy k in the separating shear layer is the deficiency of the model; k grows too slowly to cause the boundary layer to be turbulent and reattach on time. The main idea proposed by [5] is to allow the intermittency function to exceed 1 wherever the laminar boundary layer separates. This will lead to large production of k and hence allow k to grow rapidly to accelerate the transition or reattachment.

In order to invoke this idea, a criterion to locate the laminar separation should be introduced. Consider the series of velocity profiles of the Falkner-Skan boundary layer in Fig. 6. The parameter yU''/U' (blue curves) will have a positive region in adverse pressure gradients and become large if the flow separates. It does not involve turbulence variables and hence may be a good parameter to locate laminar separation. Replacing U' by an invariant of mean velocity gradient, $|S|$, the parameter becomes $d \cdot (\mathbf{n}_w \cdot \nabla|S|)/|S|$, where d is the wall distance and $\mathbf{n}_w$ is the unit normal vector of the wall. d and $\mathbf{n}_w$ are evaluated by locating the point on the wal closest to each grid point. $|S|$ is defined as $\sqrt{S_{ij}S_{ji}}$ so that $\sqrt{2}|S|$ equals to $|\partial_y U|$ in parallel flows. The final form of parameter that is used is

$$R_s \equiv d \cdot \frac{\mathbf{n}_w \cdot \nabla|S|\omega}{\sqrt{2}|S|^2}. \tag{2.10}$$

This is actually the parameter described above multiplied by $\omega/(\sqrt{2}|S|)$. The extra factor increases R_s in the separated layer.

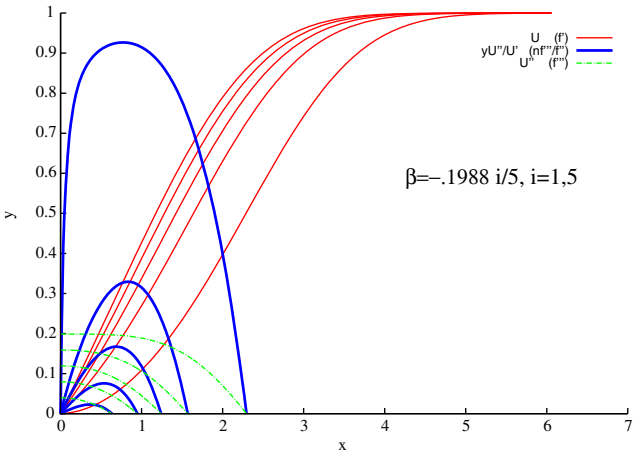

Fig. 6 The blue curve evaluates yU''/U' for Falkner-Skan boundary layer profiles. The pressure gradient parameter $\beta = -0.1988$ is just before separation. x-axis: coordinate normal to the wall; y-axis: velocity and functions of its derivative

The effective intermittency function γ_{eff} prescribed in (2.11) is the present modification to the intermittency function γ for predicting transition by laminar separation.

$$\gamma_{eff} = \max\left[\gamma, \min\left(2, F_{R_t} F_{R_v} F_{R_s}\right)\right]. \tag{2.11}$$

This modification involves 3 factors defined as follows,

$$F_{R_t} = e^{-(R_t/10)^3}, \tag{2.12}$$

$$F_{R_v} = \max\left(R_v - 200, 0\right), \tag{2.13}$$

$$F_{R_s} = \min\left[1.0, \max\left(10 + 5R_s, 0\right)\right] \times \min\left[1.0, \max\left(10 - 5R_s, 0\right)\right], \tag{2.14}$$

They are functions of R_t, R_v, and R_s, respectively. Linear ramps are again used as in the source and sink terms. The test case chosen to evaluate the model is a flat plate separation flow which has been simulated in both [15] and [7] using direct numerical simulation (DNS) and large eddy simulation (LES) respectively. F_{R_s} as defined above serves as a factor to locate the separation and switch on and off the modification. In separation flow, F_{R_s} is positive between the layers where $|S| = 0$ and $\mathbf{n}_w \cdot \nabla|S| = 0$. The influence of the lower bound of R_s for the ramp up is shown in Fig. 8. As to the upper bound of the ramp down, values greater than 2 affect very little since R_s itself has an upper bound. F_{R_v} is used for both triggering the modification and representing its strength. As is shown in Fig. 7, a higher threshold, $R_{slbound}$, for R_v causes later the reattachment. When $R_{slbound} = 0$ the modification is active only below the inflection point and reattachment is not seen (Fig. 8).

F_{R_t} plays the role of removing the modification in the free-stream. Figure 9 displays the distribution of γ_{eff} along with the contour of stream-wise velocity around a separated region. γ_{eff} is greater than 1 after the separation point, and becomes unity when the flow is fully turbulent. Before the separation point, γ_{eff} is close to zero in the boundary layer. It exceeds unity only within a thin region around the separation bubble to achieve

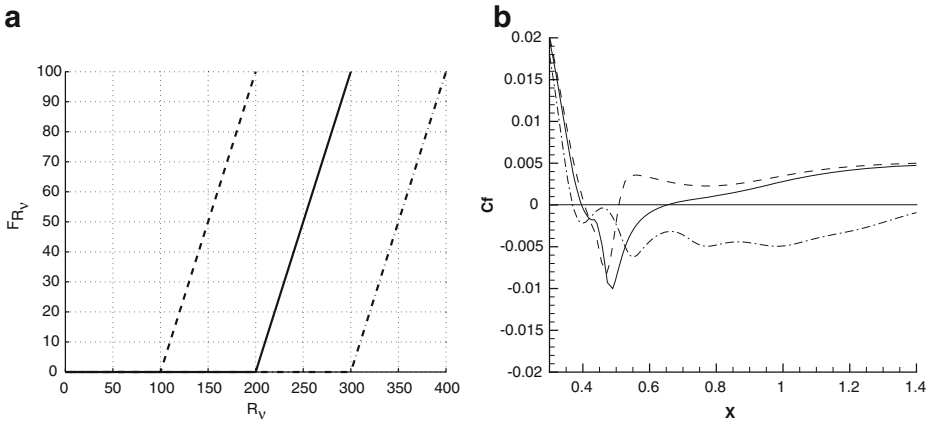

Fig. 7 Linear ramps for F_{R_v}. $R_{vlbound} = 200$ (solid); $R_{vlbound} = 100$ (dash) and too early reattachment is seen; $R_{vlbound} = 300$ (dash-dot) and no reattachment is seen

the reattachment. It appears to be a good parameter to represent the separation-induced transition.

2.5 Revision of the $k - \omega$ model

The current formulation is applied to the $k - \omega$ RANS closure [14]. The production term of the k equation is multiplied by γ_{eff}. This is the only appearance of γ within the turbulence model.

$$\frac{Dk}{Dt} = P_k - C_\mu k\omega + \partial_j\Big[\Big(\nu + \frac{\nu_T}{\sigma_k}\Big)\partial_j k\Big], \tag{2.15}$$

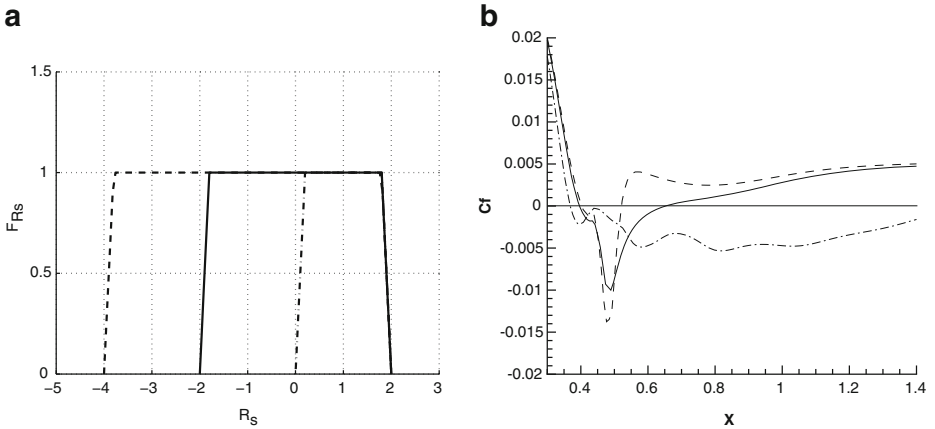

Fig. 8 Linear ramps for F_{R_s}. $R_{slbound} = -2$ (solid); $R_{slbound} = -4$ (dash) and too early reattachment is seen; $R_{slbound} = 0$ (dash-dot) and no reattachment is seen

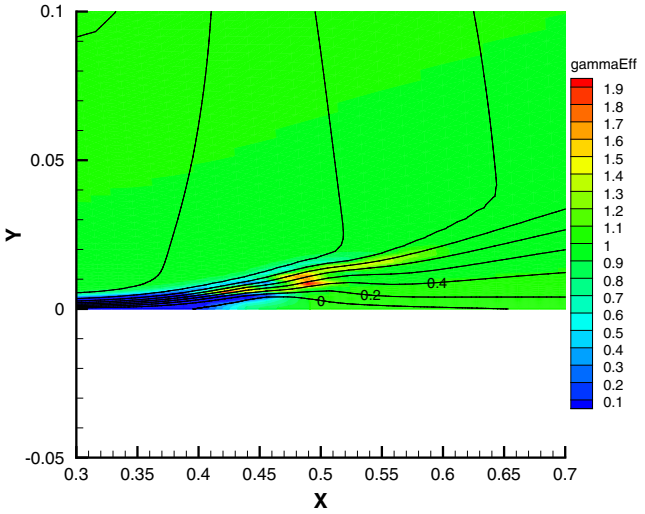

Fig. 9 Distribution of γ_{eff} and line contours of U_x around the separation bubble for the flat plate separation test case

$$P_k = \min\left(2\nu_T|S|^2, k|S|/\sqrt{3}\right)\gamma_{eff}, \tag{2.16}$$

$$\frac{D\omega}{Dt} = 2C_{\omega1}|S|^2 - C_{\omega2}\omega^2 + \partial_j\left[\left(\nu + \frac{\nu_T}{\sigma_\omega}\right)\partial_j\omega\right], \tag{2.17}$$

where $C_\mu = 0.09,\ C_{\omega1} = 5/9,\ C_{\omega2} = 3/40$ and $\sigma_\omega = \sigma_k = 2$. The eddy viscosity ν_T is k/ω. Non-zero γ will diffuse into the boundary layer, allowing k to be produced, thereby creating eddy viscosity and further enhancing the diffusion of γ. In this way, transition occurs by penetration of free-stream turbulence into the boundary layer via molecular and turbulent diffusion.

The rational of the limiter for the production term in (2.16) is explained in [2]. It is to fix the stagnation-point anomaly of turbulence kinetic energy. For example, in some cases, like flow around a blade leading edge, the limiter can avoid unphysically large levels of k near the stagnation-point.

3 Computation and Results

3.1 Flat plate cases

Test cases in this section are the T3A-C experiments reported by ERCOFTAC. Cases T3A and T3B have zero stream-wise pressure gradients with different turbulence intensities. Note that another case, T3A-, is not included in the present work. It has low free-stream turbulence intensity (0.9%). According to the classification of transition in [5], it tends to be orderly transition instead of bypass transition. The model in [3] works for T3A- in a boundary layer computation, but the current model predicts early transition for this case. Cases T3C1-5 combine the influences of free-stream turbulence and favorable/adverse pressure gradients imposed by flow in a converging/expanding channel. The main difference between

the various T3C test cases is the free-stream velocity, and hence the Reynolds number (T3C1 is an exception, which has high free-stream turbulence intensity and slow turbulence decay).

Two different domains are used. Both are two dimensional (2D). One is for the zero pressure gradient test cases (T3A and T3B). It is comprised of a flat plate wall with a length of $1.5m$ and a symmetric flat top surface with height of $0.8m$. The inlet surface is at $0.04m$ upstream of the plate leading edge to eliminate an ambiguous specification of free-stream conditions. The narrow bottom surface between the inlet and the plate leading edge is set as a symmetric boundary. The inlet boundary has uniformly fixed-value velocity, U_{in}, turbulent kinetic energy, k_{in}, specific dissipation rate, ω_{in} and zero pressure gradient. The outlet boundary has zero-gradient U, k, and ω along with zero pressure (the reference pressure). A grid-independence check was performed, and a mesh of 160 (stream-wise) $\times$ 100 (wall-normal) found to be sufficient. The first neighbor node to the wall is located at $y^+ \approx 1.0$ in the turbulent region. Values of $y^+(1) = 0.05, 0.1, 0.5$ and 1.0, have been tested. The results are not notably sensitive when $y^+(1) \leqslant 1.0$. The wall-normal grid expansion ratio is 1.1, and the stream-wise grid expansion ratio from the leading edge is 1.05, which is consistent with Fig. 10. The same expansion ratios are adopted for the mesh of the T3C cases (Fig. 11).

For the varying pressure gradient test cases (T3C series), the domain consists of a flat plate bottom wall with length of 1.65 m and a slip top wall with variable height. At the entrance, the gap between the upper and bottom walls is 0.3 m and the height varies along the stream-wise direction corresponding to the experiment. The length of the bottom surface between the inlet and the leading edge is $0.15m$ and again is set as a symmetry boundary. Boundary types of inlet and outlet are the same as those of the zero pressure gradient cases. A mesh of 230 (stream-wise) $\times$ 125 (wall-normal) is used. The first spacing is set to be $y^+ \approx 0.1$ in the turbulent region. For $y^+ > 0.5$, noticeable delay of transition will happen. The upper contour is determined by an explicit expression offered in [12]. The upper contour of T3C4 is different from the other T3C cases creating a different pressure gradient. Moreover, the length of the plate for T3C4 is $2.00m$, longer than other cases, because in this case transition occurs very close to the exit in the experimental data. Extension of the numerical domain guarantees the source term works upstream of the new exit (Fig. 11).

The SIMPLE algorithm for steady flow is applied to solve all the partial differential equations. Numerical discretization of second order accuracy is employed. These numerical setups are used for all the other test cases, as well. The fluid density ρ and the molecular viscosity μ are $1.2\,kg/m^3$ and $1.8\times10^{-5}\,kg/m{\cdot}s$, respectively. Then the kinematic viscosity $\nu = \mu/\rho = 1.5 \times 10^{-5}\,m^2s^{-1}$. The Reynolds number, Re_x, is based on the length from the

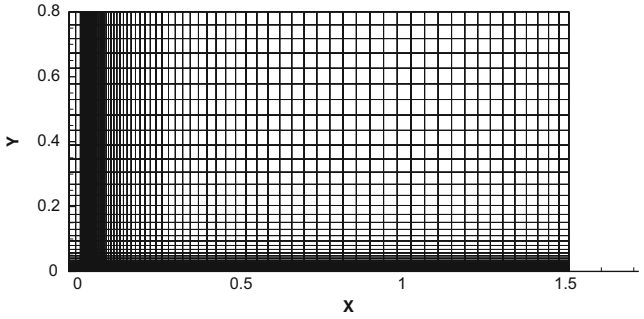

Fig. 10 Mesh used to compute T3A and T3B, showing every other line in x and y

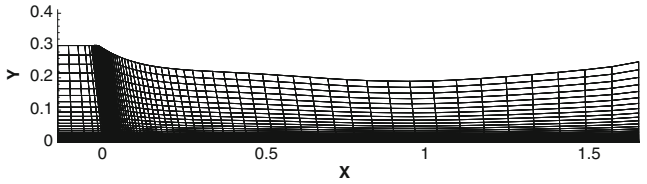

Fig. 11 Mesh used to compute T3C series, showing every other line in x and y

leading edge and local free-stream velocity. The inlet velocity, U_{in}, is specified to match the data. The inlet turbulent kinetic energy k_{in} is obtained from the measured turbulent intensity:

$$Tu_{in} = \frac{\sqrt{2/3k_{in}}}{U_{ref}}, \tag{2.17}$$

where U_{ref} equals to U_{in} in zero-pressure-gradient cases, but to local free-stream velocity in varying-pressure-gradient cases. The inlet viscosity ratio, R_t, is used to calculate and specify the inlet specific dissipation rate, ω_{in},

$$\omega_{in} = \frac{k_{in}}{R_t \nu}. \tag{2.17}$$

Both Tu_{in} and R_t are determined by agreement with the data for decay of the free-stream turbulence intensity. Figures 12, 13 and 14 show the free-stream velocity and turbulence intensity for the T3 series. Good agreement between simulations and the experimental data has been obtained by using inlet conditions in Table 1.

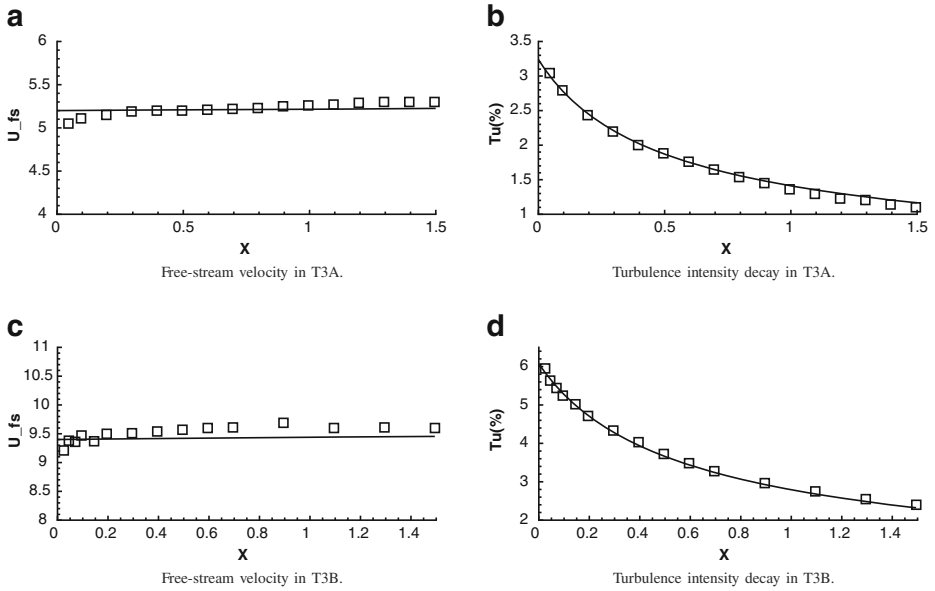

Fig. 12 Free-stream velocity and turbulence intensity in T3A and T3B cases. Experiment data (symbols), simulation results (lines)

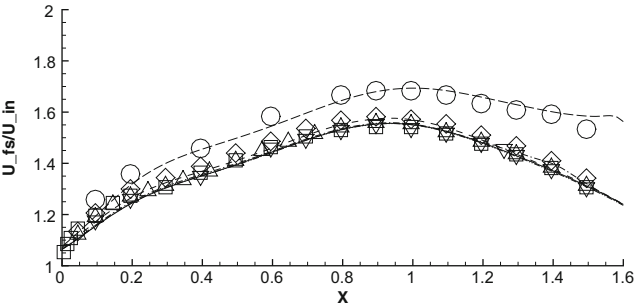

Fig. 13 Normalized free-stream velocity in T3C cases. Experiment data (symbols), simulation results (lines). The circle symbol and long-dash line refer to case T3C4, and the other T3C cases collapse together

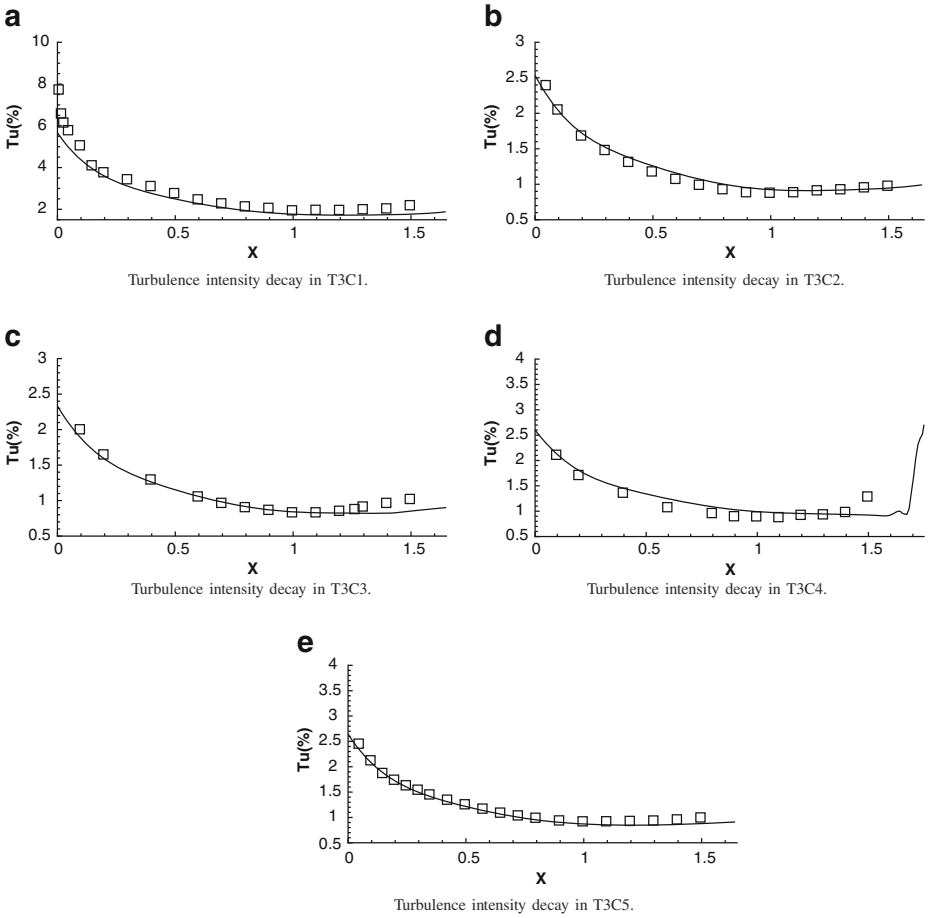

Fig. 14 Free-stream turbulence intensity in T3C cases. Experiment data (symbols), simulation results (lines)

Table 1 Summary of inlet conditions for flat plate cases

Case	$U_{in}(m/s)$	$Tu_{in}(\%)$	R_t	$\nu(\times 10^{-5} m^2 s^{-1})$
T3A	5.2	3.5	14	1.5
T3B	9.4	6.5	100	1.5
T3C1	6.0	10.0	50	1.5
T3C2	5.0	3.7	12	1.5
T3C3	3.8	3.4	8	1.5
T3C4	1.2	3.5	3.5	1.5
T3C5	8.6	4.3	17	1.5

There is experimental evidence that both turbulence time-scale and intensity affect bypass transition, i.e. the results are sensitive to the free-stream, or inlet, conditions. Computations with the current model illustrate this.

Skin friction curves computed with the same inlet dissipation rate (ω_{in}) and with varying turbulence intensity are shown in Fig. 15a. Note that $k \propto Tu^2$, with other conditions unchanged: the greater the intensity, the greater the kinetic energy. As we can see from the figure, increasing Tu accelerates transition.

Skin friction curves computed with the same $Tu = 3.5\%$ and with different ω_{in} are displayed in Fig. 15b. Decreasing ω_{in} makes turbulent energy decay more slowly and increases the eddy viscosity in the free stream. Both effects accelerate transition, and vice versa.

Contours of intermittency function, γ, near the wall for zero pressure gradient cases are displayed in Fig. 16a and c for T3A and T3B, respectively. Due to the effect of the sink term, γ decreases rapidly to zero near wall right after the leading edge. With the diffusion of γ from high values inside the free-stream to low values within the laminar boundary layer, transition is initiated: the sink term starts to decrease, with the source term switching on. Around the transition location, γ increases to one and the boundary layer becomes

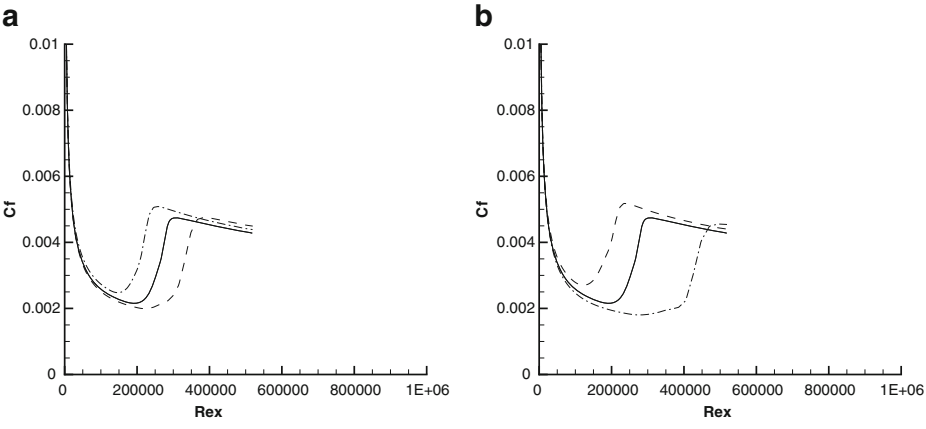

C_f curves for Tu=3.0 (dash), Tu=3.5 (solid), Tu=4.0 (dash-dot).

C_f curves for proper ω_{in} times 0.5 (dash), proper ω_{in} (solid), proper ω_{in} times 2 (dash-dot).

Fig. 15 Sensitivity to inlet k and ω (test case: T3A)

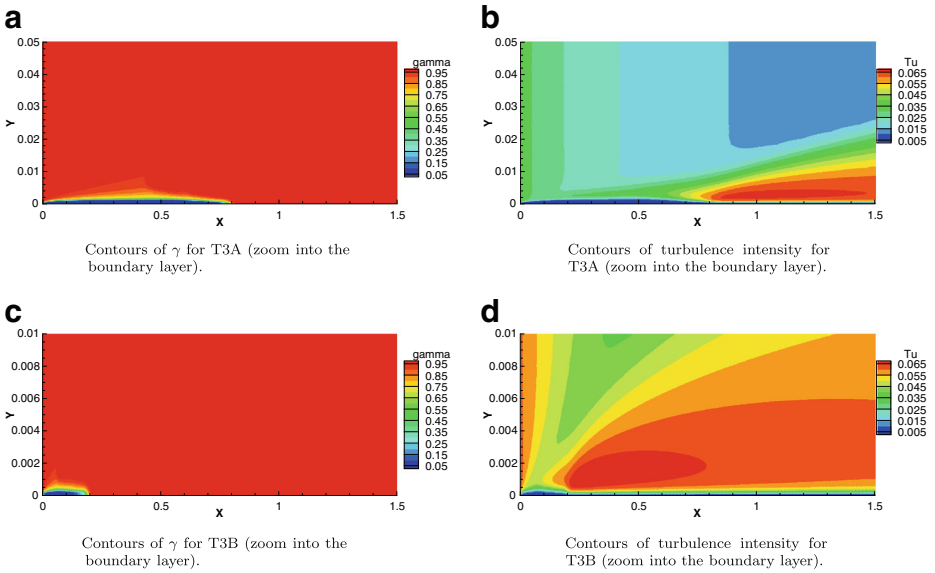

Contours of γ for T3A (zoom into the boundary layer).

Contours of turbulence intensity for T3A (zoom into the boundary layer).

Contours of γ for T3B (zoom into the boundary layer).

Contours of turbulence intensity for T3B (zoom into the boundary layer).

Fig. 16 Contours of intermittency function and turbulence intensity for T3A and T3B

turbulent. Figures 16b and d present contours of turbulent kinetic energy k. Within the transition region, k starts to grow from zero and reaches the turbulent level when transition is complete.

The computed skin friction coefficient for the T3A case is compared with the experimental data in Fig. 17a. The Blasius boundary layer solution and turbulent boundary layer correlation are also plotted. The simulation result is in decent agreement with the measured data. The laminar region is slightly above the data and the transition part of the curve is a little sharper than the data. In the words, the onset location of transition is a bit late and

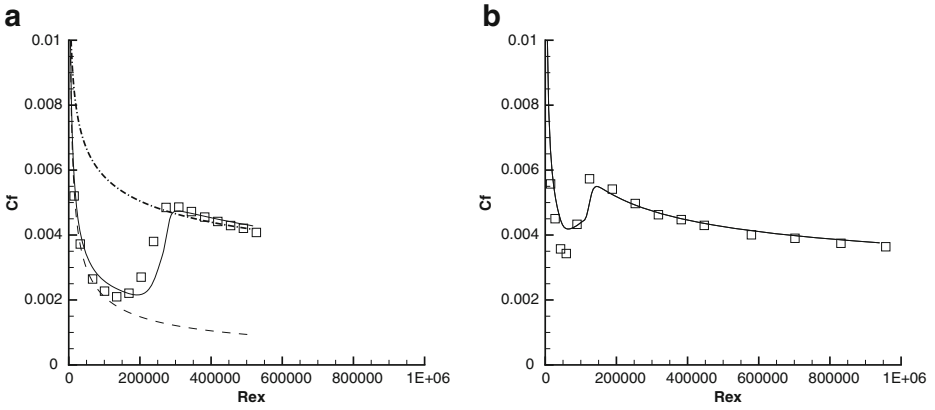

Skin friction for T3A. Experimental (symbols), laminar (dash), turbulent (dash-dot), simulation (solid).

Skin friction for T3B. Experimental (symbols), simulation (solid).

Fig. 17 Skin friction for T3A and T3B

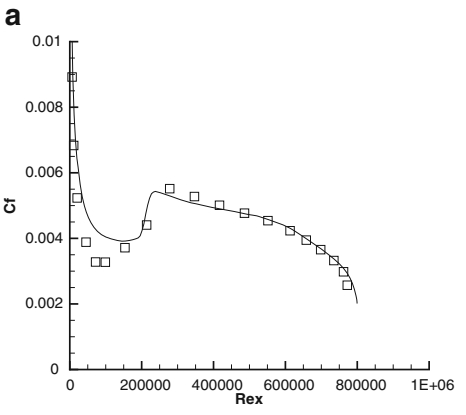

Skin friction for T3C1.

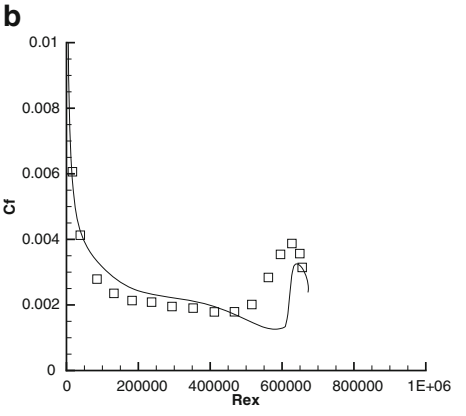

Skin friction for T3C2.

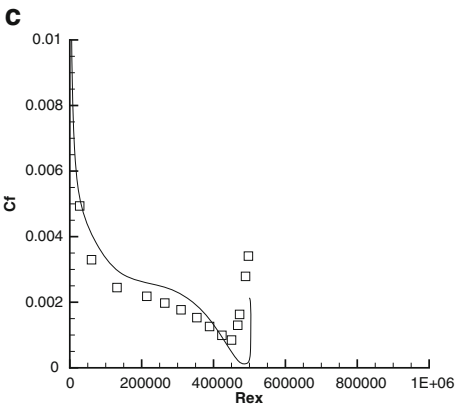

Skin friction for T3C3.

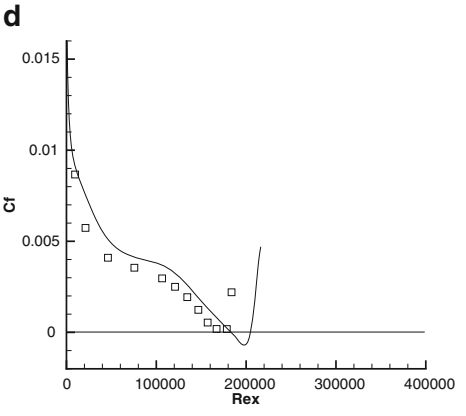

Skin friction for T3C4.

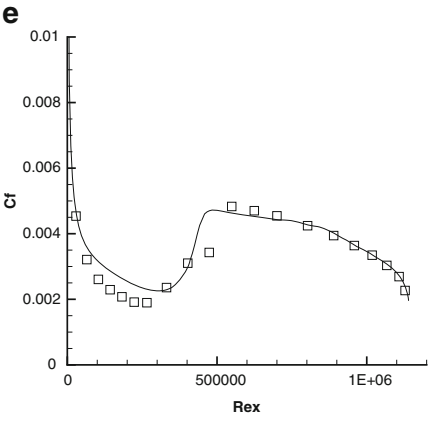

Skin friction for T3C5.

Fig. 18 C_f versus Re_x in T3C cases. Experiment data (symbols), simulation results (lines)

the transition length is therefore short as it reaches the fully turbulent region on time. This behavior exists in all the other T3 cases.

The computed skin friction coefficient for T3B is compared with the experimental data in Fig. 17b. Due to the high turbulence intensity, the skin friction before the completion of transition is over-predicted. But it does make an improvement compared with results in [6]. The minimum skin friction obtained by the current model is close to 0.004 while results of other models are just around 0.005.

The T3C test cases can be classified into two groups. T3C1 is a high free-stream turbulence level case (at first data point $Tu \approx 8.0\%$) and the other T3C cases are moderate free-stream turbulence level cases (first data point with $Tu \approx 2.5\%$).

Like T3B, with high free-stream turbulence intensity, the skin friction for T3C1 shown in Fig. 18a is better than the result of [12]. The smallest skin friction is closer to the experimental data.

The results for T3C2 are shown in Fig. 18b. In this case, the transition occurs in the adverse pressure gradient region because of the low Reynolds number. The onset location of transition is a bit late. But as mentioned above, the fast transition makes it up and meets the turbulent region at almost the same Reynolds number as measured.

The case T3C3 has even later transition than T3C2 as displayed in Fig. 18c, because its Reynolds number is smaller and the turbulence decay is faster than T3C2. In addition, it is getting closer to separation. Both of these are predicted by the current model with acceptable agreement with the data, though late transition is predicted again.

T3C4 is regarded as a benchmark for separation-induced transition in [6] and [12]. However, the location of transition onset is very close to the exit according to the experimental data, which have only one point after transition. Another problem is that the data show a very tiny separation region. Even if this case is not proper to test a model for transitional separated flow, due to these two drawbacks, Fig. 18d still shows that the current model is able to predict the transition and reattachment with an acceptable error compared with the data. A better case of flat plate separated flow from [7] is invoked to test the separation modification to the basic model in Section 3.2.

Figure 18e presents the skin friction coefficient computed by the current model for the T3C5 case. Transition occurs before the throat of the flow channel, *i.e.* within the favorable pressure gradient region, since the inlet velocity and therefore the Reynolds number is high. Because of the strong favorable pressure gradient, the transition length is extended to some extent. The model approximately predicts the behavior with small difference from the experimental data.

3.2 Flat plate separated flow

This test case was firstly studied experimentally by [8], then via DNS by [15] and via LES by [7]. The current model is able to predict locations of transition and reattachment with decent accuracy compared to the LES data of [7]. The inlet is set at one half 'chord' length L upstream of the leading edge. But the plate length in the present work is extended to the computational exit, $X/L = 1.5$, in order to allow a fully turbulent region downstream and uniform pressure at the exit. For simplicity, X/L is replaced with X in the following plots. The contour of the upper wall is exactly as [7]. The bottom surface from the inlet to the leading edge is specified as a symmetric boundary, and after the leading edge, it is a non-slip wall boundary to the outlet. The whole top surface is a slip wall boundary. Uniform profiles for U_{in}, k_{in} and ω_{in} are specified at the inlet. The Reynolds number, based on the chord length L and the inflow velocity U_{in} is 60,000. k_{in} and ω_{in} are again determined to

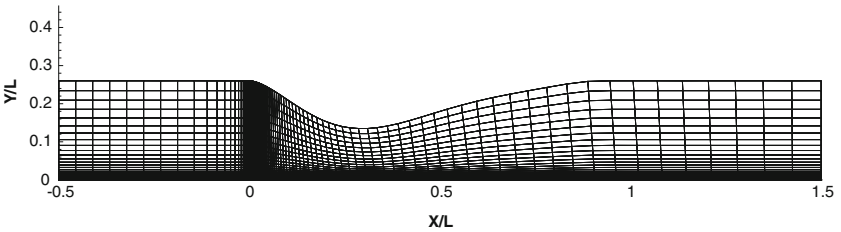

Fig. 19 Mesh for flat plate separated flow case showing every other line in x and y

match the decay of the free-stream turbulence intensity of the LES data. At the outlet, zero gradient is used for most of the variables except p, which has uniform, zero value. The 2D mesh for this case, shown in Fig. 19, is 200 (stream-wise) $\times$ 80 (wall-normal), with first grid spacing $y^+ \approx 0.1$ in the turbulent region. A mesh finer than this has little effect on the results.

Two simulations with different free-stream turbulence intensities are performed. The higher the free-stream turbulence intensity is, the earlier the transition and reattachment will be. Details about the inlet conditions are listed in Table 2. Figure 20 shows the free-stream turbulence intensity distributions for these two simulations. The reference velocity to define Tu is the local free-stream velocity. Though the inlet Tu is different from the LES data, the present simulations reproduce the levels of Tu after the leading edge, which is at $X = 0$.

The pressure distribution and skin friction on the wall for Simulation 1 are displayed in Fig. 21. The reference pressure is the exit pressure, and the reference velocity is simply U_{in} for both C_p and C_f. There should be a sudden increase of pressure and a pressure plateau in the separated region, but the current model does not predict the plateau very clearly. And also the smallest pressure is under estimated by the model. The level of C_f at the beginning of the turbulent region is under-predicted, but this is attributable to the $k-\omega$ model. The intermittency model transits to full turbulence after the flow reattaches, but the $k-\omega$ model itself cannot predict the correct level of C_f in the turbulent region.

The location of separation and reattachment simulated by the current model is relatively accurate, though the transition occurs a bit early. This again leads to the observation that the nature of transition in a separated boundary layer is different from attached flow, bypass transition. The former has an inflection point while the latter does not. It is difficult to simulate such a complicated case very accurately by using a simple RANS model since the transition in this case may be induced by various mechanisms. However, the current model is a considerable improvement on the original $k-\omega$ RANS model, which is shown by the dash-dot curve in Fig. 21b.

Figure 22 depicts the contours of stream-wise mean velocity computed both by LES and the current model. The separation bubble produced by the model is thiner than that of LES.

The skin friction coefficient of Simulation 2 is plotted in Fig. 23. Similar to simulation 1, the model predicts the locations of separation and reattachment with good

Table 2 Summary of inlet conditions for the flat plate separated flow case

Case	$U_{in}(m/s)$	$Tu_{in}(\%)$	$\omega_{in}(s^{-1})$	$\nu(\times 10^{-5} m^2 s^{-1})$
Simulation 1	0.9	5.8	90	1.5
Simulation 2	0.9	7.5	60	1.5

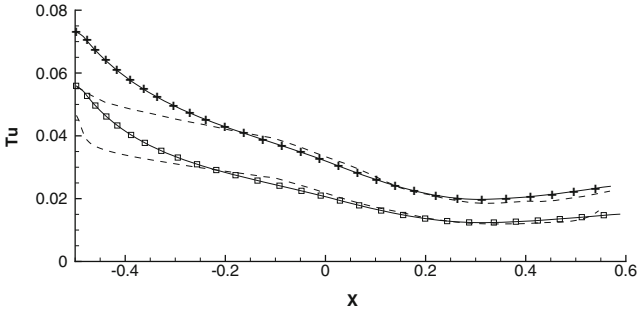

Fig. 20 Distributions of free-stream turbulence intensity for the flat plate separated flow case. "Simulation 1" (□), "Simulation 2" (+); current model (solid), LES by [7] (dash)

agreement with the LES data, but the transition location and the turbulence level are not accurate. In addition, comparing the results shown both in Figs. 21b and 23, the difference between the two C_f curves of the model is slight, whereas that of the LES data is noticeable. This means that the results based on the model are not sensitive to the free-stream turbulence intensity except for an earlier reattachment in Simulation 2, which has higher free-stream Tu.

3.3 Compressor blade cascade

In this section, a 2D flow through a compressor blade passage with two different free-stream turbulence intensities is simulated by the current model and the results are compared with the DNS data in [16].

The computational domain with the grid is shown in Fig. 24. The coordinates of the blade are based on a NACA 65 [16]. The mesh is 223 (stream-wise) × 286 (wall-normal)

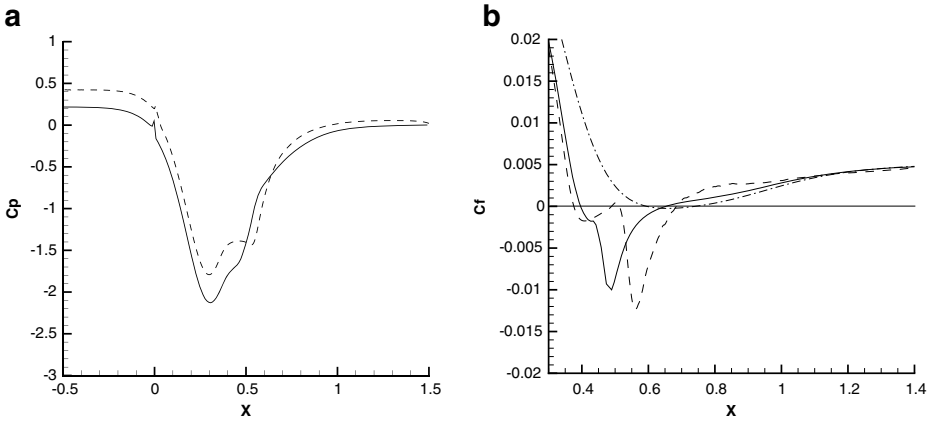

Pressure coefficient. Current model (solid), LES by Lardeau et al (2012) (dash).

Skin friction. Current model (solid), LES by Lardeau et al (2012) (dash), $k-\omega$ model (dash-dot).

Fig. 21 Plots for Simulation 1

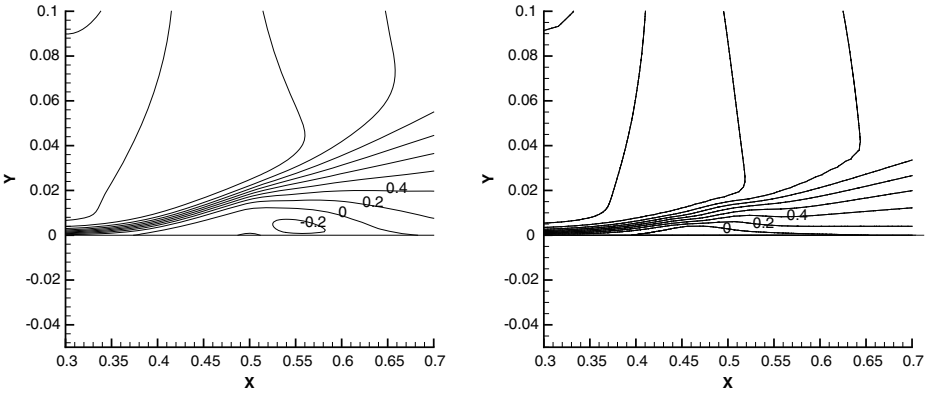

Fig. 22 Contours of stream-wise velocity around the separation bubble for Simulation 1

with the first grid spacing y^+ ranging from 0.1 to 1.0. To simulate the compressor blade cascade, periodic boundary conditions upstream and downstream of the blade surface are used. The periodic surfaces are specified at $X/L < 0$ and $X/L > 1$, where the axial chord L is selected as the reference length scale. A non-slip boundary condition is applied on the blade surfaces. The blade pitch, i.e. the height of the inlet and outlet is $P = 0.59L$. The inlet is located at $X/L = -0.5$, and the outlet is extended to $X/L = 2$. For simplicity, X/L is denoted as X below. At the inlet boundary, uniform U_{in}, k_{in} and ω_{in} are specified to produce the desired free-stream mean velocity and turbulence decay. The angle between

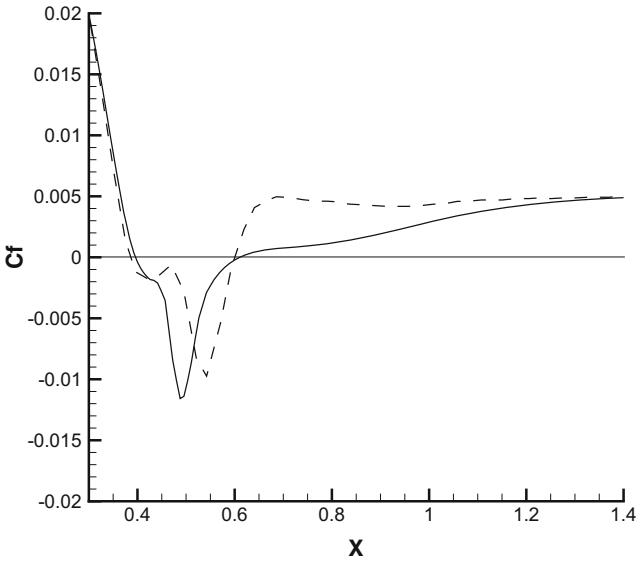

Fig. 23 Skin friction for Simulation 2. Current model (solid), LES by [7] (dash)

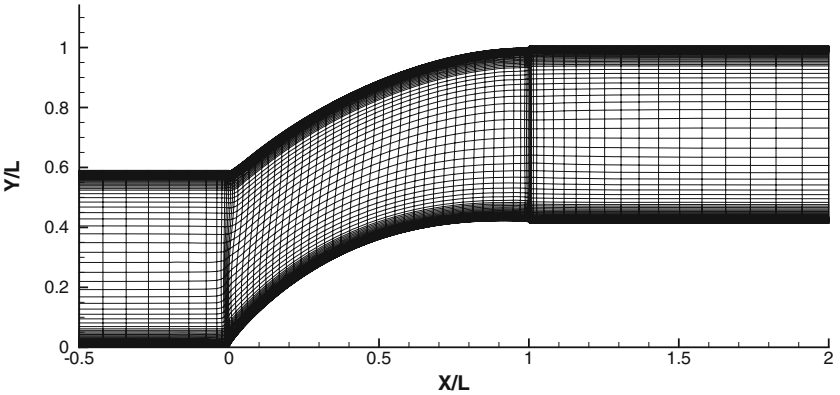

Fig. 24 Mesh for compressor blade cascade case showing every third line in x and y

the inlet mean velocity vector and the horizontal axis is $\alpha = 42°$. The Reynolds number based on U_{in} and L is 138,500. The outlet boundary condition is the same as the other cases described above.

Table 3 gives values of variables at the inlet for both simulations. The corresponding contours of the turbulence intensity are displayed in Fig. 25. These are similar to distributions of Tu obtained by [16]. The values of Tu at the mid-pitch follows the DNS data from the leading edge to the trailing edge, which reproduces the same free-stream turbulence intensity as Cases T2 and T3 in [16]. Pressure coefficient and skin friction on the surfaces of the blade are plotted in Figs. 26 and 27 for both simulations. The reference pressure is at the leading edge and the reference velocity equals U_{in}.

In the separated region of Simulation 1, the model does not produce an obvious pressure plateau and then a sudden pressure rise as the DNS data on the suction surface, even though the negative skin friction by the model extends farther than the DNS. The onsets of transition are later and the lengths of transition are longer than DNS data on both surfaces.

The most significant issue for Simulation 2 is the unphysically separated region on the suction surface predicted by the current model (Fig. 27d). The transition occurs too late to keep the flow attached. Note that transition on the suction surface occurs in an adverse pressure gradient region, which tends to cause late transition by the current model. On the pressure side, the location and length of transition appear close to the DNS data, whereas the laminar level of the skin friction is higher.

With higher free-stream turbulence intensity, transition occurs earlier and the length of transition becomes shorter, which illustrates that the current model is able to prediect the sensitivity to the free-stream turbulence intensity for this case.

For both simulations, the turbulent levels are lower than the DNS data. But again this is caused by the original turbulence model as can been seen in the figures. After transition,

Table 3 Summary of inlet conditions for the compressor blade cascade case

Case	$U_{in}(m/s)$	$Tu_{in}(\%)$	$\omega_{in}(s^{-1})$	$\nu(\times 10^{-5} m^2 s^{-1})$
Simulation 1	2.0775	9.0	130	1.5
Simulation 2	2.0775	11.0	100	1.5

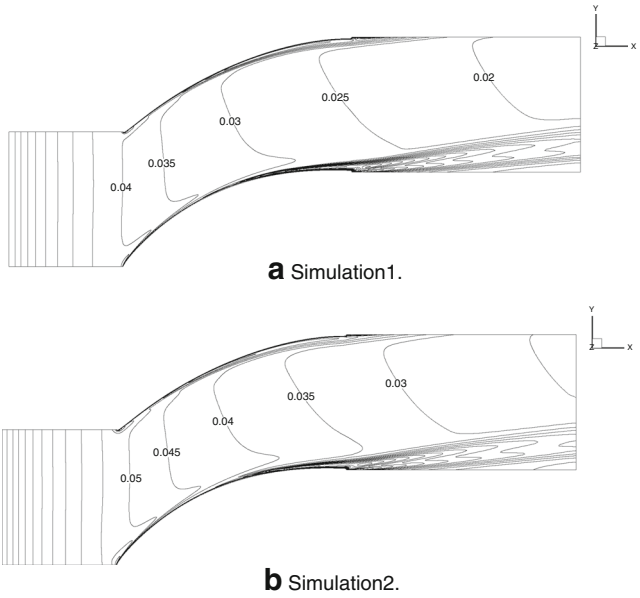

Fig. 25 Contours of turbulence intensity for both simulations

the computations shifts to pure $k-\omega$ and C_f reaches the identical turbulent level predicted by $k-\omega$ model. One can infer that the current model for bypass transition may work fine if the $k-\omega$ RANS model were able to predict the fully turbulent region of this flow more accurately. In other words, benefit is indeed gained when this intermittency model is applied to the $k-\omega$ model even for such a challenging case.

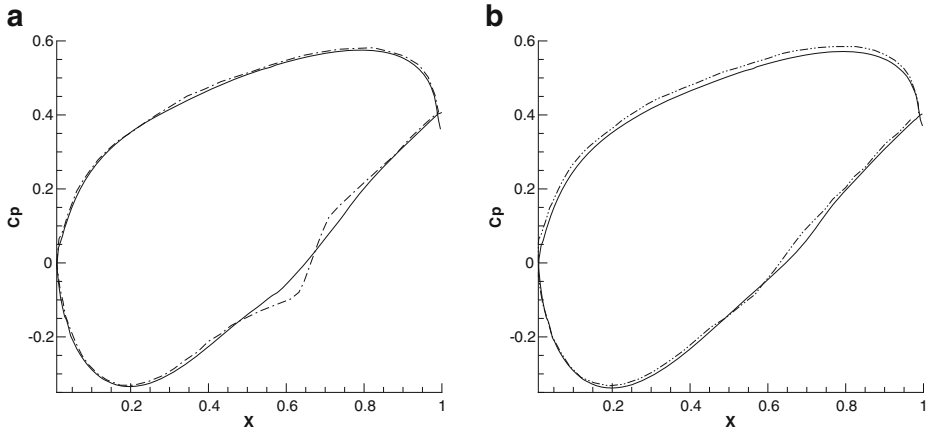

Pressure coefficient for Simulation 1. Current model (solid), DNS (dash-dot).

Pressure coefficient for Simulation 2. Current model (solid), DNS (dash-dot-dot).

Fig. 26 Pressure coefficient of the compressor blade case

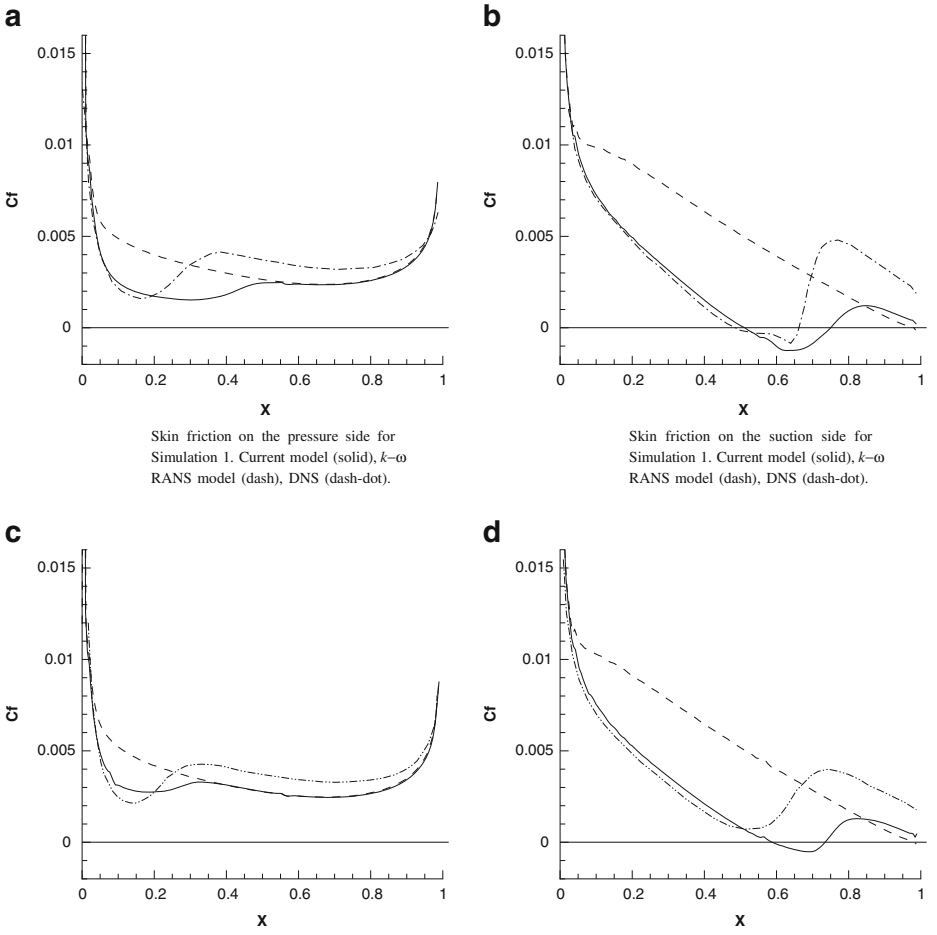

Skin friction on the pressure side for Simulation 1. Current model (solid), k–ω RANS model (dash), DNS (dash-dot).

Skin friction on the suction side for Simulation 1. Current model (solid), k–ω RANS model (dash), DNS (dash-dot).

Skin friction on the pressure side for Simulation 2. Current model (solid), k–ω RANS model (dash), DNS (dash-dot-dot).

Skin friction on the suction side for Simulation 2. Current model (solid), k–ω RANS model (dash), DNS (dash-dot-dot).

Fig. 27 Skin friction of the compressor blade case

4 Conclusions

The objective of the present work is to propose an intermittency bypass transition model that is simpler than those published and without data correlation. Although it remains quite empirical, the number of parameters is fewer and the role of each more apparent. The model is based on only one intermittency transport equation. Transition is initiated by diffusion and a source term carries it to turbulence. A sink term is applied to ensure a laminar boundary layer before transition and it vanishes in the turbulent region. Moreover, this model is suitable for general computational fluid dynamics applications.

A range of test cases have been computed to validate the current model. The numerical results show decent agreement with the experimental or DNS data with different free-stream Reynolds numbers, turbulence intensities and pressure gradients. The model does

not depend directly on pressure gradient and is capable of predicting separation-induced transition and reattachment in a strong adverse pressure gradient region. The limitations of the current model include late transition in the adverse pressure gradient region and inapplicability to cases with low free-stream turbulence intensity ($Tu < 1\%$). Because of the nature of the model, it is mainly proposed to simulate bypass transition. The model is not suitable for cases with transition by instability waves.

Acknowledgments This work was funded by NSF grant #CBET-1228195. We are grateful to Dr. Sylvain Lardeau for willingly providing his LES data.

References

1. Dhawan, S., Narasimha, R.: Some properties of boundary layer during the transition from laminar to turbulent flow motion. J. Fluid Mech. **3**, 418–436 (1958)
2. Durbin, P.A., Pettersson-Reif, B.A.: Statistical theory and modeling for turbulent flows. 2nd edn. Wiley (2011)
3. Durbin, P.A.: An intermittency model for bypass transition. Int. J. Heat Fluid Flow **36**, 1–6 (2012)
4. Durbin, P.A., Wu, X.: Transition beneath vortical disturbances. Annu. Rev. Fluid Mech. **39**(1), 107–128 (2007)
5. Langtry, R.B.: A correlation-based transition model using local variables for unstructured parallelized cfd codes. PhD thesis, Universitat Stuttgart, Holzgartenstr. 16, 70174 Stuttgart (2006)
6. Langtry, R.B., Menter, F.R.: Correlation-based transition modelling for unstructured parallelized computational fluid dynamics codes. AIAA J. **47**(12), 2894–2906 (2009)
7. Lardeau, S., Leschziner, M.A., Zaki, T.A.: Large eddy simulation of transitional separated flow over a flat plate and a compressor blade. Flow Turbul. Combust. **88**(1–2), 19–44 (2012)
8. Lou, W., Hourmouziadis, J.: Separation bubbles under steady and periodic-unsteady main flow conditions. J. Turbomach. **122**, 634–643 (2000)
9. Menter, R.F., Langtry, R.B., Volker, S.: Transition modelling for general purpose cfd codes. Flow Turbul. Combus. **77**(1-4), 277–303 (2006)
10. Praisner, T.J., Clark, J.P.: Predicting transition in turbomachinery, part 1: a review and new model development. J. Turbomach. **129**, 1–13 (2007)
11. Steelant, J., Dick, E.: Modelling of bypass transition with conditioned navierstokes equations coupled to an intermittency transport equation. Int. J. Numer. Methods Fluids **23**(3), 193–220 (1996)
12. Suluksna, K., Dechaumphai, P., Juntasaro, E.: Correlations for modeling transitional boundary layers under influences of freestream turbulence and pressure gradient. Int. J. Heat Fluid Flow **30**(1), 66–75 (2009)
13. Suzen, Y.B., Huang, P.G.: Modeling of flow transition using an intermittency transport equation. J. Fluids Eng. **122**(2), 273–284 (2000)
14. Wilcox, D.: Turbulence Modeling for CFD. DCW inc. (1993)
15. Wissink, J.G., Rodi, W.: Direct numerical simulations of transitional flow in turbomachinery. J. Turbomach. **128**, 668 (2006)
16. Zaki, T.A., Wissink, J.G., Rodi, W., Durbin, P.A.: Direct numerical simulations of transition in a compressor cascade: the influence of free-stream turbulence. J. Fluid Mech. **665**, 57–98 (2010)